Sensitivity analysis for observables of the chiral magnetic effect using a multiphase transport model

Ling Huang,[1,2,3] Mao-Wu Nie,[4,5,*] and Guo-Liang Ma[3,1,†]

[1]*Shanghai Institute of Applied Physics, Chinese Academy of Sciences, Shanghai 201800, China*
[2]*University of Chinese Academy of Sciences, Beijing 100049, China*
[3]*Key Laboratory of Nuclear Physics and Ion-beam Application (MOE), Institute of Modern Physics, Fudan University, Shanghai 200433, China*
[4]*Institute of Frontier and Interdisciplinary Science, Shandong University, Qingdao 266237, China*
[5]*Key Laboratory of Particle Physics and Particle Irradiation, Ministry of Education, Shandong University, Qingdao, Shandong, 266237, China*

(Received 4 July 2019; revised manuscript received 20 December 2019; accepted 11 February 2020; published 28 February 2020)

Because the traditional observable of charge-dependent azimuthal correlator γ contains contributions from both the chiral magnetic effect (CME) and its background, a new observable of R_{Ψ_m} was recently proposed which is expected to be able to distinguish the CME from the background. In this study, we apply two methods to calculate R_{Ψ_m} using a multiphase transport model without or with introduction of a percentage of CME-induced charge separation. Our results show that the shape of final R_{Ψ_2} distribution is flat for the case without the CME, but concave for that with an amount of the CME because the initial CME signal survives from strong final state interactions. By comparing the responses of R_{Ψ_2} and γ to the strength of the initial CME signal, we observe that both observables show nonlinear sensitivities to the CME because of the existence of strong final state interactions.

DOI: 10.1103/PhysRevC.101.024916

I. INTRODUCTION

Relativistic heavy-ion collisions provide us a unique way to explore the nature of quark gluon plasma (QGP) experimentally [1,2]. In order to probe the QGP, many observables have been studied experimentally, such as jet quenching [3–5] and collective flow [6–9]. Recently, the chiral magnetic effect (CME) was proposed as a good observable which reveals some topological and electromagnetic properties of the QGP. In the early stage of relativistic heavy-ion collisions, an extremely large magnetic field can be created which can induce an electric current along the strong magnetic field for chirality imbalanced domains with a nonzero topological charge inside the QGP, i.e., the chiral magnetic effect [10–14]. The transitional observable to detect the CME is a charge-dependent azimuthal correlator, $\gamma = \langle\cos(\phi_\alpha + \phi_\beta - 2\Psi_{RP})\rangle$, which has been widely investigated both experimentally and theoretically [15–21]. Unfortunately, the observable cannot distinguish the CME signal from the large background clearly [22–29], because many kinds of backgrounds can contribute to γ [25,27]. Recently, a new observable, namely the shape of R_{Ψ_m}, has been proposed to be a more sensitive probe to search for the CME signal. Many studies of the R_{Ψ_m} observable have been reported [30–34]. For examples, some studies show that the shape of the R_{Ψ_m} distribution is convex due to background but concave due to the CME [31,32], but another study shows that R_{Ψ_m} could be also concave due to the background only [34]. Therefore, the effectiveness and practicability of the new observable R_{Ψ_m} are still being debated. On the other hand, because the lifetime of magnetic field may be quite short due to the limited conductivity of QGP [35–37], it is questionable whether the CME signal formed in the early stage can survive from strong final state interactions since relativistic heavy-ion collisions actually involves many final dynamic evolution stages. It has been found out that a multiphase transport model (AMPT) is a good way to study the interplay between the CME and final state interactions in relativistic heavy-ion collisions [38–40]. Ma *et al.* [38] demonstrated that a 10% initial charge separation due to the CME can describe experimental data of the γ correlator in Au+Au collisions at 200 GeV, but only 1–2% of charge separation can remain finally due to strong final state interactions. In this study, we investigate the new observable of R_{Ψ_m} with two versions of the AMPT model: the original AMPT model which contains backgrounds only and the AMPT model with not only backgrounds but also a CME-induced charge separation. We compare the shapes of R_{Ψ_m} distributions from the pure background case and the CME case with background. We also study the relationship between the strength of the CME between R_{Ψ_m} and γ in order to reveal the sensitivities of the two observables to the CME.

This paper is organized as follows. We will introduce our methods of calculating R_{Ψ_m} and how to introduce a CME-induced charge separation into the AMPT model in Sec. II. Our results and discussion are presented in Sec. III.

*maowu.nie@sdu.edu.cn
†glma@fudan.edu.cn

II. MODEL AND CALCULATION METHOD

A. The AMPT model

A multiphase transport model, AMPT, has been extensively used to investigate the physics of relativistic heavy-ion collisions [41–46]. In order to study the observable R_{Ψ_m}, we simulated Au+Au collisions at 200 GeV with the new version of the AMPT model with a string melting mechanism. There are four main stages in the AMPT model [41]: the initial conditions, parton cascade, conversion from partonic to hadronic matter, and hadronic rescatterings. The initial conditions mainly simulate the spatial and momentum distributions of minijet partons from QCD hard processes and soft string excitations by using the HIJING model [47,48]. The parton cascade describes strong interactions among partons through elastic partonic collisions only which are controlled by a partonic interaction cross section (we chose it to be 3 mb.) [49]. When all partons stop interacting, the AMPT model simulates hadronization by coalescence, i.e., converting two nearest partons into a meson and three nearest quarks into a baryon. Finally, the relativistic transport model (ART) model is used to simulate baryon-baryon, baryon-meson, and meson-meson reactions in hadronic rescatterings [50]. In our calculations, we use the newest version in which we have fixed the problem of the violation of charge conservation [51] by fixing all hadronic reaction channels. Since there is no chiral magnetic effect in the original AMPT model, we need to introduce an additional CME-induced charge separation into the initial conditions in order to study the CME-related physics. In a previous work [38], the CME signal was successfully introduced into the AMPT model by switching the p_y values of a percentage of the downward moving u ($\bar{d}$) quarks with those of the upward moving $\bar{u}$ (d) quarks to thus produce a charge dipole separation in the initial conditions. In this work, we follow the same procedure. In our convention, we always choose the x axis along the direction of impact parameter b from the target center to the projectile center, the z axis along the beam direction, and the y axis perpendicular to the x and z directions. The percentage of initial charge separation is used to adjust strength of the CME. The percentage f is defined as

$$f = \frac{N^{+(-)}_{\uparrow(\downarrow)} - N^{+(-)}_{\downarrow(\uparrow)}}{N^{+(-)}_{\uparrow(\downarrow)} + N^{+(-)}_{\downarrow(\uparrow)}}, \tag{1}$$

where N is the number of a given species of quarks, $+$ and $-$ denote positive and negative charges, respectively, and $\uparrow$ and $\downarrow$ represent their directions of movement along the y axis. Note that the relation between our f and a_1 is $f = (4/\pi)a_1$, where a_1 is the coefficient of $\sin\phi$ term in the Fourier expansion of the particle azimuthal angle distribution. By taking advantage of two settings of AMPT model, i.e. without and with introduction of the CME, we next will apply the new observable R_{Ψ_m} to systemically investigate how it works for searching for the CME.

B. Calculation methods

Two methods, the mixing-particle method [30] and the shuffling-particle method [31], are used to calculate the new observable of R_{Ψ_m} for Au+Au collisions at 200 GeV (30–50%). Because the definition of R_{Ψ_m} is based on another observable C_{Ψ_m}, we first show the formulas for calculating C_{Ψ_m} in the mixing-particle method as follows [30]:

$$\langle S_{p^+}\rangle = \frac{1}{N_p}\sum_1^{N_p} \sin\left(\frac{m}{2}(\phi_p^+ - \Psi_m)\right), \tag{2}$$

$$\langle S_{n^-}\rangle = \frac{1}{N_n}\sum_1^{N_n} \sin\left(\frac{m}{2}(\phi_n^- - \Psi_m)\right), \tag{3}$$

$$\Delta S = \langle S_{p^+}\rangle - \langle S_{n^-}\rangle, \tag{4}$$

where ϕ is the azimuthal angle of a particle, Ψ_m is the mth-order event reaction plane, superscript $+$ and $-$ signs indicate the particles' charges, and N_p and N_n represent the total number of positive and negative charged particles, respectively. For $m = 2$, the distribution of ΔS is expected to be broadened due to the existence of the CME.

In the mixing-particle method, to make a corresponding reference of ΔS, which is denoted as $\Delta S_{\rm mix}$, we select the same number of particles as for ΔS but ignore their charges, and we can do similar calculations as follows:

$$\langle S_{p^{\rm mix}}\rangle = \frac{1}{N_p}\sum_1^{N_p} \sin\left(\frac{m}{2}(\phi_p^{\rm mix} - \Psi_m)\right), \tag{5}$$

$$\langle S_{n^{\rm mix}}\rangle = \frac{1}{N_n}\sum_1^{N_n} \sin\left(\frac{m}{2}(\phi_n^{\rm mix} - \Psi_m)\right), \tag{6}$$

$$\Delta S_{\rm mix} = \langle S_{p^{\rm mix}}\rangle - \langle S_{n^{\rm mix}}\rangle. \tag{7}$$

where we use superscript "mix" to sign mixing particles' charges. Then we can get C_{Ψ_m} by taking the ratio of the distribution of ΔS [$N(\Delta S)$] and the distribution of $\Delta S_{\rm mix}$ [$N(\Delta S_{\rm mix})$]:

$$C_{\Psi_m}(\Delta S) = N(\Delta S)/N(\Delta S_{\rm mix}), \quad m = 2, 3, \ldots. \tag{8}$$

On the other hand, by shifting the Ψ_m to $\Psi_m + \pi/m$, $C^{\perp}_{\Psi_m}(\Delta S)$ is expected to only reflect the background of the CME. We replace Ψ_m with $\Psi_m + \pi/m$ in the above formulas; $C^{\perp}_{\Psi_m}(\Delta S)$ can be obtained as follows:

$$\langle S^{\perp}_{p^+}\rangle = \frac{1}{N_p}\sum_1^{N_p} \sin\left[\frac{m}{2}\left(\phi_p^+ - \Psi_m - \frac{\pi}{m}\right)\right], \tag{9}$$

$$\langle S^{\perp}_{n^-}\rangle = \frac{1}{N_n}\sum_1^{N_n} \sin\left[\frac{m}{2}\left(\phi_n^- - \Psi_m - \frac{\pi}{m}\right)\right], \tag{10}$$

$$\Delta S^{\perp} = \langle S^{\perp}_{p^+}\rangle - \langle S^{\perp}_{n^-}\rangle, \tag{11}$$

$$\langle S^{\perp}_{p^{\rm mix}}\rangle = \frac{1}{N_p}\sum_1^{N_p} \sin\left[\frac{m}{2}\left(\phi_p^{\rm mix} - \Psi_m - \frac{\pi}{m}\right)\right], \tag{12}$$

$$\langle S^{\perp}_{n^{\rm mix}}\rangle = \frac{1}{N_n}\sum_1^{N_n} \sin\left[\frac{m}{2}\left(\phi_n^{\rm mix} - \Psi_m - \frac{\pi}{m}\right)\right], \tag{13}$$

$$\Delta S^{\perp}_{\rm mix} = \langle S^{\perp}_{p^{\rm mix}}\rangle - \langle S^{\perp}_{n^{\rm mix}}\rangle, \tag{14}$$

$$C^{\perp}_{\Psi_m}(\Delta S) = N(\Delta S^{\perp})/N(\Delta S^{\perp}_{\rm mix}), \quad m = 2, 3, \ldots. \tag{15}$$

In the other method, the shuffling-particle method, the formulas are same as those of mixing-particle method except

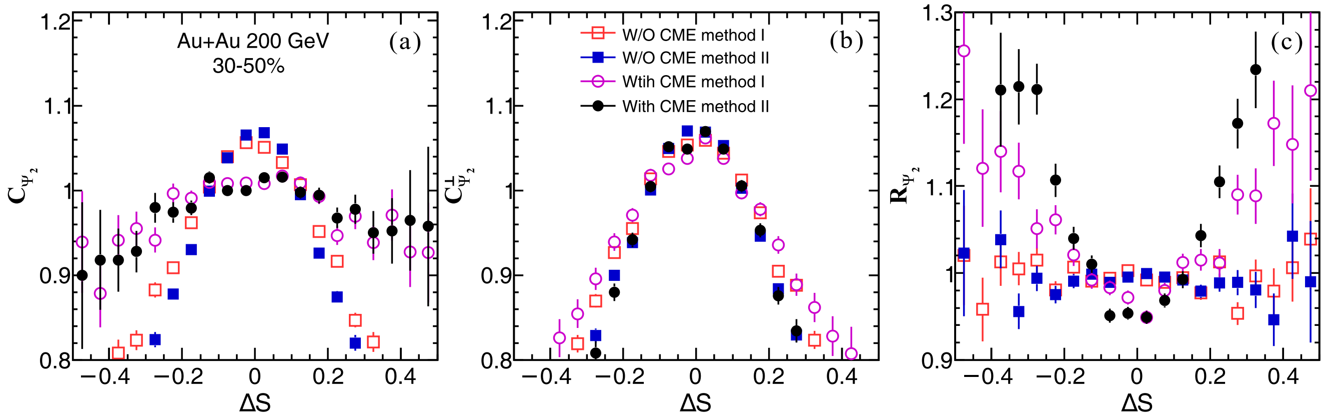

FIG. 1. C_{Ψ_2}, $C^{\perp}_{\Psi_2}$, and R_{Ψ_2} in Au+Au collisions at 200 GeV (30–50%) from the AMPT model without or with the CME based on two different methods, where method I and method II represent the mixing-particle method and the shuffling-particle method, respectively.

for the definitions of $\Delta S_{\rm mix}$ and $\Delta S^{\perp}_{\rm mix}$. In the above mixing-particle method, $\Delta S_{\rm mix}$ and $\Delta S^{\perp}_{\rm mix}$ are obtained by ignoring charges when mixing all particles. But in the shuffling-particle method, they are obtained by reshuffling the charges of charged particles, denoted as $\Delta S_{\rm shuffle}$ and $\Delta S^{\perp}_{\rm shuffle}$. The two methods have the same goal to eliminate any charge-related correlation when selecting particles by either ignoring or reshuffling charges, which are expected to provide a good background reference since all selected particles are charge-blind from a same event.

For both methods, once we get $C_{\Psi_m}(\Delta S)$ and $C^{\perp}_{\Psi_m}(\Delta S)$, $R_{\Psi_m}(\Delta S)$ [31,32,34] is obtained as

$$R_{\Psi_m}(\Delta S) = C_{\Psi_m}(\Delta S)/C^{\perp}_{\Psi_m}(\Delta S). \tag{16}$$

The shape of $R_{\Psi_m}(\Delta S)$ is expected to be sensitive to whether the CME exists or not. In our work, we will calculate $R_{\Psi_m}(\Delta S)$ with the two methods with the AMPT model without and with introduction of a CME-induced charge separation, and the detailed results will be presented in Sec. III.

III. RESULTS AND DISCUSSIONS

In this work, we selected particles with transverse momenta $0.35 < p_T < 2.0$ GeV/c and pseudorapidity $-1.0 < \eta < 1.0$ to calculate C_{Ψ_m}, $C^{\perp}_{\Psi_m}$, and R_{Ψ_m}. As for Ψ_m, the information of coordinate space in the initial stage is used for its reconstruction [52]. Two methods are both applied for calculating R_{Ψ_m}. The results are presented in Sec. III A. In order to investigate the relationship between R and the CME strength, the dependences of the CME observables on initial charge separation percentage have also been calculated, and are presented Sec. III B.

A. C_{Ψ_2}, $C^{\perp}_{\Psi_2}$, and R_{Ψ_2}

Since the original AMPT model does not include the CME, we can calculate R_{Ψ_2} through it to study the pure background effect. On the other hand, R_{Ψ_2} from the AMPT model that introduces the CME can help us find the CME signal apart from the background. The results are presented in Fig. 1, which shows C_{Ψ_2}, $C^{\perp}_{\Psi_2}$, and R_{Ψ_2} from the AMPT model without or with introduction of an initial CME-induced charge separation based on two methods, where method I denotes the mixing-particle method and method II denotes the shuffling-particle method. We found that our results from the two methods are consistent with each other. For the original AMPT model without the CME, C_{Ψ_2} and $C^{\perp}_{\Psi_2}$ are convex, and R_{Ψ_2} is flat, in terms of their shapes. On the other hand, for the

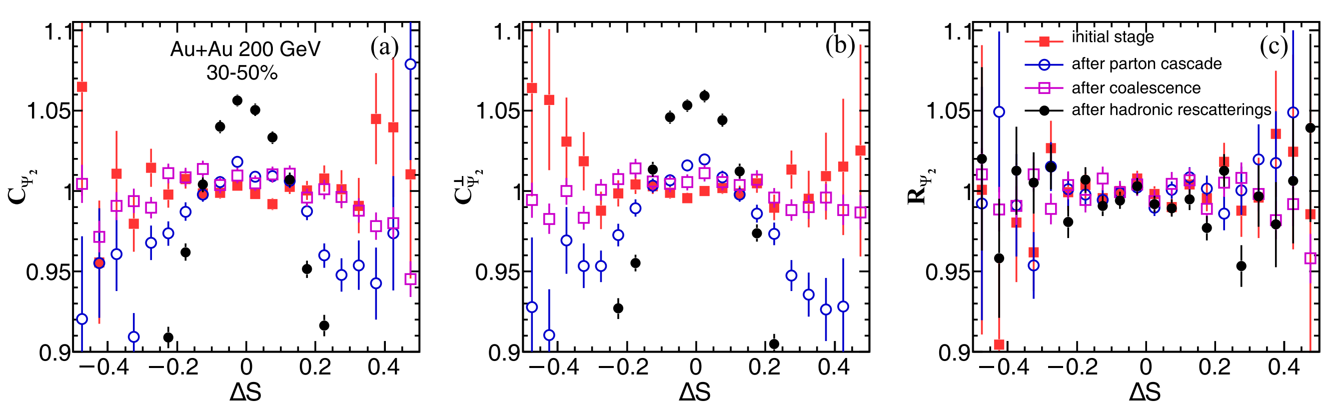

FIG. 2. C_{Ψ_2}, $C^{\perp}_{\Psi_2}$, and R_{Ψ_2} in Au+Au collisions at 200 GeV (30–50%) for different evolution stages of the original AMPT model without the CME.

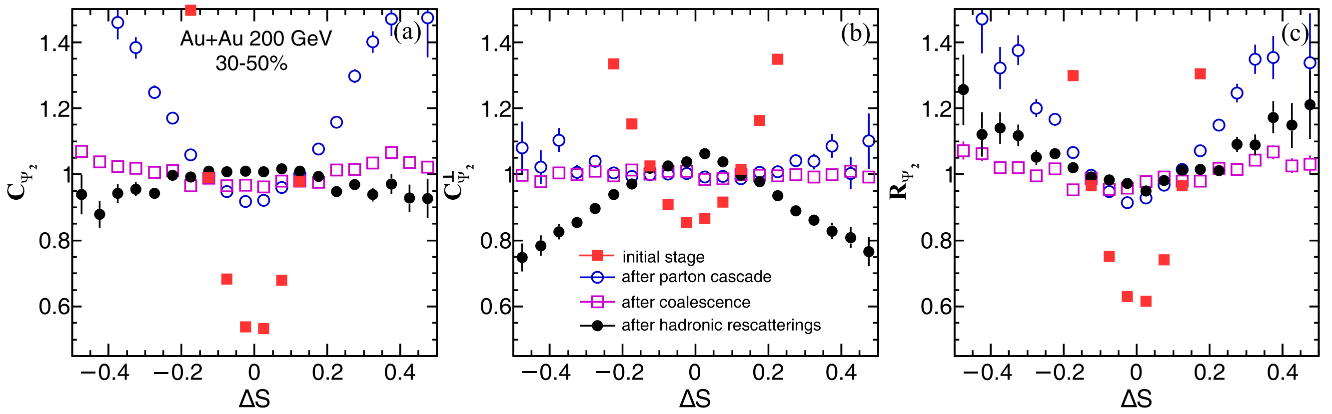

FIG. 3. C_{Ψ_2}, $C^{\perp}_{\Psi_2}$, and R_{Ψ_2} in Au+Au collisions at 200 GeV (30–50%) from different evolution stages of the AMPT model with a 10% initial CME-induced charge separation.

AMPT model with introduction of a 10% of CME-induced initial charge separation, C_{Ψ_2} and $C^{\perp}_{\Psi_2}$ are convex, and they are broadened differently due to the CME which makes the shape of R_{Ψ_2} concave finally. From Fig. 1, our results show that C_{Ψ_2} and $C^{\perp}_{\Psi_2}$ are convex no matter whether there is the CME or not. However, our R_{Ψ_2} is flat with background only, but it becomes concave when introducing a 10% initial CME-induced charge separation.

From the results in Fig. 1, we can see R_{Ψ_2} can be a probe to distinguish the CME signal from the background. To understand why R_{Ψ_2} can work for searching for the CME, we further study the stage evolution of C_{Ψ_2}, $C^{\perp}_{\Psi_2}$, and R_{Ψ_2} for the four stages of heavy-ion collisions in the AMPT model. The results of original AMPT without the CME are presented in Fig. 2. We can see that C_{Ψ_2}, $C^{\perp}_{\Psi_2}$ are flat at the initial stage, and then convex at the stage after parton cascade. After the coalescence, C_{Ψ_2} and $C^{\perp}_{\Psi_2}$ both tend to be flat, but they become more convex after hadronic rescatterings. However, as the ratio of C_{Ψ_2} and $C^{\perp}_{\Psi_2}$, R_{Ψ_2} is always flat and around unity from initial stage to after hadronic rescatterings.

At the same time, we also calculated the stage evolution of C_{Ψ_2}, $C^{\perp}_{\Psi_2}$, and R_{Ψ_2} for the AMPT model with the CME. As presented in Fig. 3, C_{Ψ_2}, $C^{\perp}_{\Psi_2}$, and R_{Ψ_2} are most concave at the initial stage due to introduction of the CME. Then after parton cascade, the three results are still concave but the magnitude is weakened compared to that at initial stage, due to the strong parton cascade. At the stage of after coalescence, the three results tend to become flat. After hadronic rescatterings, C_{Ψ_2} and $C^{\perp}_{\Psi_2}$ become convex while R_{Ψ_2} becomes concave. In this way, the concave shape due to the CME survives from the final state interactions, which gives us a chance to search for the CME by using the new observable of R_{Ψ_2}. In a previous work, Ma *et al.* [38] also investigated the evolution of the γ observable in the AMPT model, which shows that final state interactions strongly weaken the initial CME-induced charge separation. Our results indicates that the CME signal in R_{Ψ_2} suffers a fate similar to that of the γ observable, i.e., the CME signal from the initial stage is weakened because of final state interactions [38]

B. C_{Ψ_3}, $C^{\perp}_{\Psi_3}$, and R_{Ψ_3}

We also study R_{Ψ_3}, which is defined with respect to the third-order event plane Ψ_3. As the direction of magnetic field is expected to be uncorrelated to Ψ_3, some research [31] indicates that R_{Ψ_3} from the background cannot identify the CME signal and background. Therefore, we calculated R_{Ψ_3} using the original AMPT model and the AMPT model

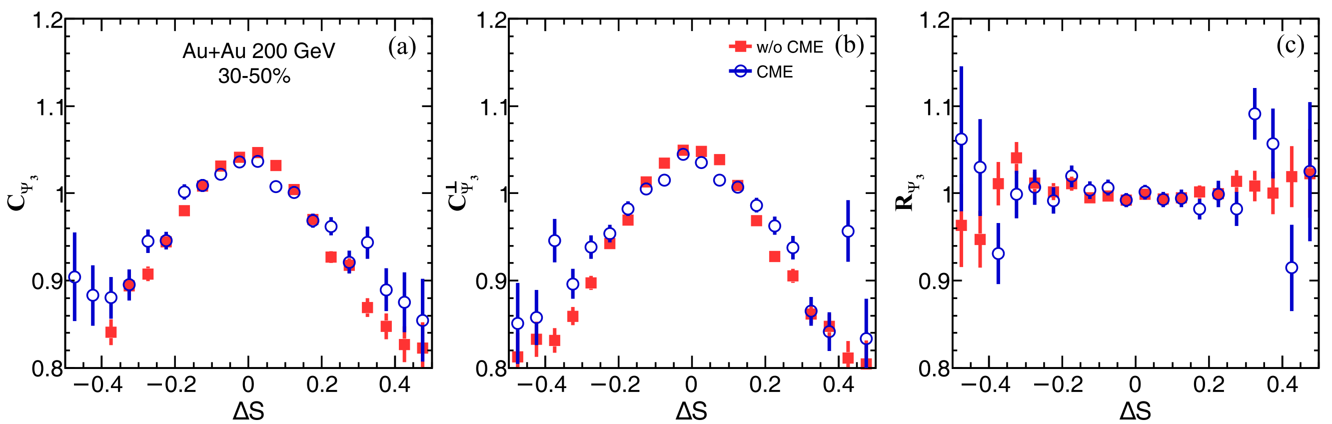

FIG. 4. C_{Ψ_3}, $C^{\perp}_{\Psi_3}$, and R_{Ψ_3} in Au+Au collisions at 200 GeV (30–50%) from the AMPT model without the CME and with a 10% initial CME-induced charge separation.

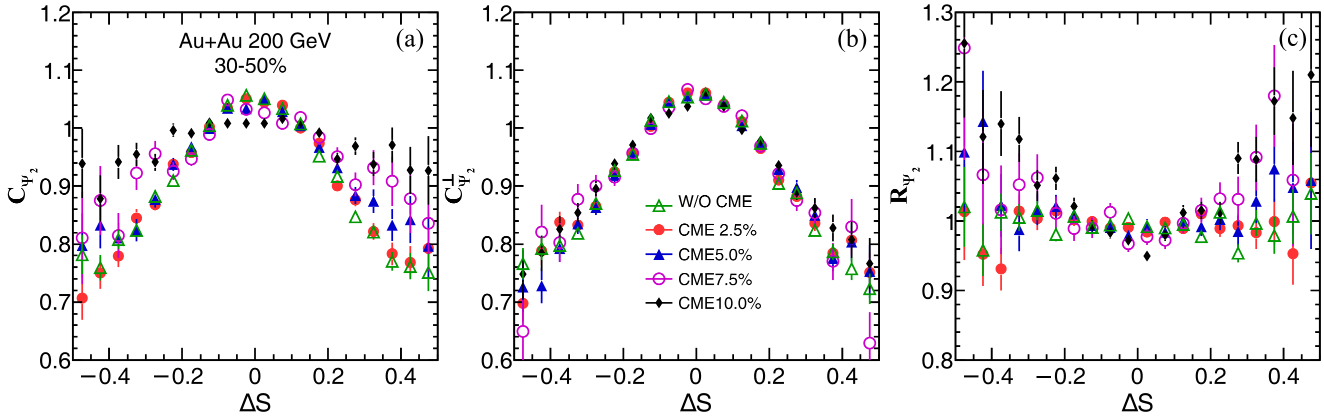

FIG. 5. C_{Ψ_2}, $C_{\Psi_2}^{\perp}$, and R_{Ψ_2} in Au+Au collisions at 200 GeV (30–50%) from the AMPT model without the CME and with different percentages of initial CME-induced charge separation.

introducing the CME. The results are shown in Fig. 4; we can see that C_{Ψ_3} and $C_{\Psi_3}^{\perp}$ are convex, R_{Ψ_3} are flat. The results from the original AMPT model are same as those from the AMPT model with the CME, which confirms that R_{Ψ_3} is indeed not sensitive to the CME.

C. Sensitivity to the CME

In previous work, Ma *et al.* [38] studied relationship between the traditional observable of γ and the initial charge separation percentage due to the CME through the AMPT model, which indicates that γ is not linearly responsive to the initial charge separation percentage when considering final state interactions. This indicates that only when the charge separation percentage is large enough, e.g., more than 5%, can the effect on γ from the CME become visible. It is interesting to also study how sensitive to the CME the new observable of R_{Ψ_2} is.

Figure 5 shows our results of C_{Ψ_2}, $C_{\Psi_2}^{\perp}$, and R_{Ψ_2} from the AMPT model with different initial charge separation percentages. The results from the original AMPT model without the CME are similar to those from the AMPT model with 2.5% initial charge separation, where R_{Ψ_2} are both flat within the error bars. When introducing a 5% initial charge separation into the AMPT model, C_{Ψ_2} become wider than the C_{Ψ_2} with 2.5% initial charge separation, which makes R_{Ψ_2} tend to be concave. With increases of the initial charge separation percentage increases, C_{Ψ_2} becomes wider and wider, and concave R_{Ψ_2} becomes narrower and narrower. Within our current event statistics (2 million events for each case), our results show that when the initial charge separation percentage is larger than 5%, the shape of R_{Ψ_2} starts to be sensitive to the CME. However, since heavy-ion experiments have many more events than our models, it is possible for experimentalists to measure an even smaller percentage of CME signal based on a larger event data sample.

In order to compare the sensitivities to the CME between γ and R_{Ψ_2}, we study how they depend on the initial charge separation percentage. In Fig. 6(a), we show that the γ and $\Delta\gamma$ have nonlinear responses to the initial charge separation

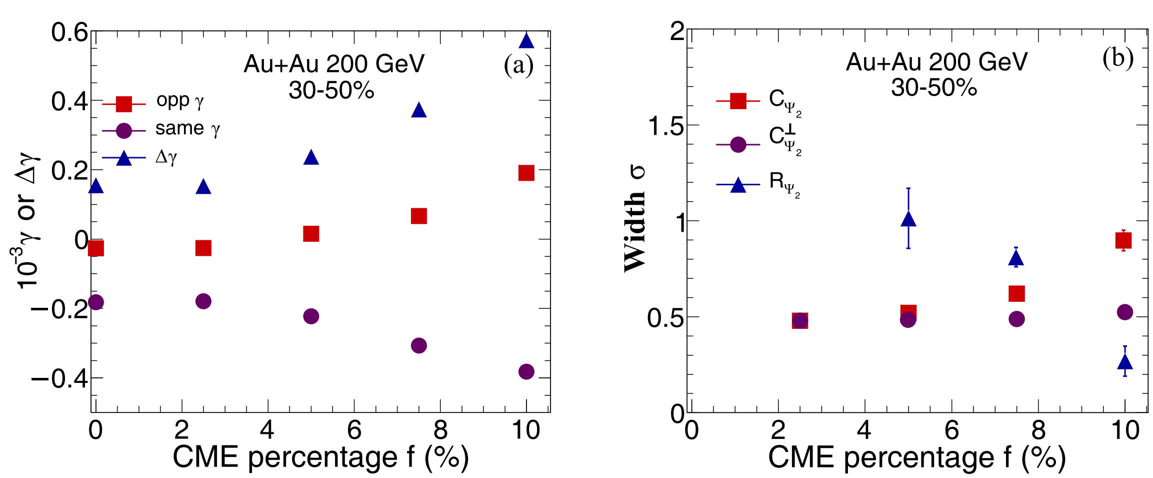

FIG. 6. The initial charge separation percentage dependences of final γ and $\Delta\gamma$ (a), and the widths of C_{Ψ_2}, $C_{\Psi_2}^{\perp}$, and R_{Ψ_2} (b) in Au+Au collisions at 200 GeV (30–50%).

percentage. The γ and $\Delta\gamma$ from the AMPT with a 2.5% initial charge separation are almost same as those from the original AMPT model (0%). γ and $\Delta\gamma$ from the AMPT model with a 5.0% initial charge separation are slightly different from those with 0% and 2.5%, which indicates it is difficult to use γ to detect the CME if the initial charge separation percentage is very small. When the initial charge separation percentage increases from 5% to 10%, the γ and $\Delta\gamma$ start to increase with the initial charge separation percentage, which is consistent with the previous results from Ma *et al.* [38]. Figure 6(b) shows the width σ of C_{Ψ_2}, $C^{\perp}_{\Psi_2}$, and R_{Ψ_2} distributions for different initial charge separation percentages in Au+Au collisions (30–50%), where we apply a Gaussian function to fit the distributions of C_{Ψ_2}, $C^{\perp}_{\Psi_2}$, and R_{Ψ_2}.We can see that the width of C_{Ψ_2} increases but that of $C^{\perp}_{\Psi_2}$ changes little, so the width of R_{Ψ_2} decreases, when the initial charge separation percentage is larger than 5%. Note that the width of R_{Ψ_2} for 2.5% is not plotted because the distribution of R_{Ψ_2} for 2.5% is so flat that we cannot extract the width by our fitting within our current event statistics. On the other hand, R_{Ψ_2} shows a flat shape for the background only, which indicates that a large number of event statistics are required to discriminate a small CME signal from the background. Through the comparison based on the current statistics, our results indicate that both γ and R_{Ψ_2} start to be sensitive when the initial charge separation percentage becomes large enough (more than $\approx$5%) since strong final state interactions suppress the initial CME signal.

IV. SUMMARY

We have studied the chiral magnetic effect with the new observable of R_{Ψ_m} within the framework of a multiphase transport model without and with inrtoduction of CME-induced charge separation. The results from the mixing-particle method and the shuffling-particle method are consistent with each other. Our results show that the shape of the R_{Ψ_2} distribution is flat for the background only, while it can be concave with some amount of CME. But R_{Ψ_3} is not sensitive to the CME. We also present the stage evolution of the R_{Ψ_2} distribution, which indicates that the initial CME signal is weakened by strong final state interactions, similarly to the traditional observable of γ. We compare the sensitivities to the CME between R_{Ψ_2} and γ, which indicates that both of them have nonlinear responses to the CME because of the existence of strong final state interactions.

ACKNOWLEDGMENTS

We thank Roy Lacey and Jiangyong Jia for their valuable discussions. This work was supported by the National Natural Science Foundation of China under Grants No. 11890714, No. 11835002, No. 11961131011, No. 11421505, the Key Research Program of the Chinese Academy of Sciences under Grant No. XDPB09 (L.H. & G.-L.M.), and the China Postdoctoral Science Foundation under Grant No. 2019M662319 (M.-W.N.).

[1] J. Adams *et al.* (STAR Collaboration), Nucl. Phys. A **757**, 102 (2005).
[2] K. Adcox *et al.* (PHENIX Collaboration), Nucl. Phys. A **757**, 184 (2005).
[3] X. N. Wang and M. Gyulassy, Phys. Rev. Lett. **68**, 1480 (1992).
[4] J. Adams *et al.* (STAR Collaboration), Phys. Rev. Lett. **91**, 172302 (2003).
[5] K. Aamodt *et al.* (ALICE Collaboration), Phys. Lett. B **696**, 30 (2011).
[6] J. Y. Ollitrault, Phys. Rev. D **46**, 229 (1992).
[7] P. Romatschke and U. Romatschke, Phys. Rev. Lett. **99**, 172301 (2007).
[8] U. Heinz and R. Snellings, Annu. Rev. Nucl. Part. Sci. **63**, 123 (2013).
[9] Z. Xu, C. Greiner, and H. Stocker, Phys. Rev. Lett. **101**, 082302 (2008).
[10] D. Kharzeev, Phys. Lett. B **633**, 260 (2006).
[11] D. Kharzeev and A. Zhitnitsky, Nucl. Phys. A **797**, 67 (2007).
[12] D. E. Kharzeev, L. D. McLerran, and H. J. Warringa, Nucl. Phys. A **803**, 227 (2008).
[13] K. Fukushima, D. E. Kharzeev, and H. J. Warringa, Phys. Rev. D **78**, 074033 (2008).
[14] K. Fukushima, D. E. Kharzeev, and H. J. Warringa, Nucl. Phys. A **836**, 311 (2010).
[15] B. I. Abelev *et al.* (STAR Collaboration), Phys. Rev. Lett. **103**, 251601 (2009).
[16] B. I. Abelev *et al.* (STAR Collaboration), Phys. Rev. C **81**, 054908 (2010).
[17] B. Abelev *et al.* (ALICE Collaboration), Phys. Rev. Lett. **110**, 012301 (2013).
[18] L. Adamczyk *et al.* (STAR Collaboration), Phys. Rev. C **88**, 064911 (2013).
[19] L. Adamczyk *et al.* (STAR Collaboration), Phys. Rev. C **89**, 044908 (2014).
[20] L. Adamczyk *et al.* (STAR Collaboration), Phys. Rev. Lett. **113**, 052302 (2014).
[21] V. Khachatryan *et al.* (CMS Collaboration), Phys. Rev. Lett. **118**, 122301 (2017).
[22] S. Schlichting and S. Pratt, Phys. Rev. C **83**, 014913 (2011).
[23] S. Pratt, S. Schlichting, and S. Gavin, Phys. Rev. C **84**, 024909 (2011).
[24] A. Bzdak, V. Koch, and J. Liao, Phys. Rev. C **81**, 031901(R) (2010).
[25] A. Bzdak, V. Koch, and J. Liao, Phys. Rev. C **83**, 014905 (2011).
[26] J. Liao, V. Koch, and A. Bzdak, Phys. Rev. C **82**, 054902 (2010).
[27] F. Wang, Phys. Rev. C **81**, 064902 (2010).
[28] A. Bzdak, V. Koch, and J. Liao, in *Strongly Interacting Matter in Magnetic Fields*, Lecture Notes in Physics Vol. 871 (Springer, Berlin, 2013), p. 503.
[29] J. Zhao, Z. Tu, and F. Wang, Nucl. Phys. Rev. **35**, 225 (2018).
[30] N. N. Ajitanand, R. A. Lacey, A. Taranenko, and J. M. Alexander, Phys. Rev. C **83**, 011901(R) (2011).
[31] N. Magdy, S. Shi, J. Liao, N. Ajitanand, and R. A. Lacey, Phys. Rev. C **97**, 061901(R) (2018).
[32] Y. Feng, J. Zhao, and F. Wang, Phys. Rev. C **98**, 034904 (2018).
[33] D. Y. Shen, J. H. Chen, G. L. Ma, Y. G. Ma, Q. Y. Shou, S. Zhang, and C. Zhong, Phys. Rev. C **100**, 064907 (2019).

[34] P. Bozek, Phys. Rev. C **97**, 034907 (2018).
[35] V. Voronyuk, V. D. Toneev, W. Cassing, E. L. Bratkovskaya, V. P. Konchakovski, and S. A. Voloshin, Phys. Rev. C **83**, 054911 (2011).
[36] W. Cassing, O. Linnyk, T. Steinert, and V. Ozvenchuk, Phys. Rev. Lett. **110**, 182301 (2013).
[37] H. T. Ding, F. Karsch, and S. Mukherjee, Int. J. Mod. Phys. E **24**, 1530007 (2015).
[38] G. L. Ma and B. Zhang, Phys. Lett. B **700**, 39 (2011).
[39] Q. Y. Shou, G. L. Ma, and Y. G. Ma, Phys. Rev. C **90**, 047901 (2014).
[40] L. Huang, C. W. Ma, and G. L. Ma, Phys. Rev. C **97**, 034909 (2018).
[41] Z. W. Lin, C. M. Ko, B. A. Li, B. Zhang, and S. Pal, Phys. Rev. C **72**, 064901 (2005).
[42] G. L. Ma and Z. W. Lin, Phys. Rev. C **93**, 054911 (2016).
[43] G. L. Ma, Phys. Rev. C **88**, 021902(R) (2013).
[44] G. L. Ma, Phys. Rev. C **89**, 024902 (2014).
[45] A. Bzdak and G. L. Ma, Phys. Rev. Lett. **113**, 252301 (2014).
[46] M. W. Nie, P. Huo, J. Jia, and G. L. Ma, Phys. Rev. C **98**, 034903 (2018).
[47] X. N. Wang and M. Gyulassy, Phys. Rev. D **44**, 3501 (1991).
[48] M. Gyulassy and X. N. Wang, Comput. Phys. Commun. **83**, 307 (1994).
[49] B. Zhang, Comput. Phys. Commun. **109**, 193 (1998).
[50] B. A. Li and C. M. Ko, Phys. Rev. C **52**, 2037 (1995).
[51] Z. W. Lin, Acta Phys. Polon. Suppl. **7**, 191 (2014).
[52] G. L. Ma and X. N. Wang, Phys. Rev. Lett. **106**, 162301 (2011).